Human Brain Imaging and Radiation Dosimetry of ^{11}C-*N-Desmethyl*-Loperamide, a PET Radiotracer to Measure the Function of P-Glycoprotein

Nicholas Seneca[1], Sami S. Zoghbi[1], Jeih-San Liow[1], William Kreisl[1], Peter Herscovitch[2], Kimberly Jenko[1], Robert L. Gladding[1], Andrew Taku[1], Victor W. Pike[1], and Robert B. Innis[1]

[1]*Molecular Imaging Branch, National Institute of Mental Health, National Institutes of Health, Bethesda, Maryland; and* [2]*PET Department, Clinical Center, National Institutes of Health, Bethesda, Maryland*

P-glycoprotein (P-gp) is a membrane-bound efflux pump that limits the distribution of drugs to several organs of the body. At the blood–brain barrier, P-gp blocks the entry of both loperamide and its metabolite, *N-desmethyl*-loperamide (*N*-dLop), and thereby prevents central opiate effects. Animal studies have shown that ^{11}C-dLop, compared with ^{11}C-loperamide, is an especially promising radiotracer because it generates negligible radiometabolites that enter the brain. The purposes of this study were to determine whether ^{11}C-dLop is a substrate for P-gp at the blood–brain barrier in humans and to measure the distribution of radioactivity in the entire body to estimate radiation exposure. **Methods:** Brain PET scans were acquired in 4 healthy subjects for 90 min and included concurrent measurements of the plasma concentration of unchanged radiotracer. Time–activity data from the whole brain were quantified using a 1-tissue-compartment model to estimate the rate of entry (K_1) of radiotracer into the brain. Whole-body PET scans were acquired in 8 healthy subjects for 120 min. **Results:** For brain imaging, after the injection of ^{11}C-dLop the concentration of radioactivity in the brain was low (standardized uptake value, ~15%) and stable after approximately 20 min. In contrast, uptake of radioactivity in the pituitary was about 50-fold higher than that in the brain. The plasma concentration of ^{11}C-dLop declined rapidly, but the percentage composition of plasma was unusually stable, with the parent radiotracer constituting 85% of total radioactivity after approximately 5 min. The rate of brain entry was low (K_1 = 0.009 ± 0.002 mL·cm^{-3}·min^{-1}; n = 4). For whole-body imaging, as a measure of radiation exposure to the entire body the effective dose of ^{11}C-dLop was 7.8 ± 0.6 μSv/MBq (n = 8). **Conclusion:** The low brain uptake of radioactivity is consistent with ^{11}C-dLop being a substrate for P-gp in humans and confirms that this radiotracer generates negligible quantities of brain-penetrant radiometabolites. In addition, the low rate of K_1 is consistent with P-gp rapidly effluxing substrates while they transit through the lipid bilayer. The radiation exposure of ^{11}C-dLop is similar to that of many other ^{11}C-radiotracers. Thus, ^{11}C-dLop is a promising radiotracer to study the function of P-gp at the blood–brain barrier, at which impaired function would allow increased uptake into the brain.

Key Words: PET; *N-desmethyl*-loperamide; P-glycoprotein

J Nucl Med 2009; 50:807–813
DOI: 10.2967/jnumed.108.058453

Received Sep. 24, 2008; revision accepted Jan. 6, 2009.
For correspondence or reprints contact: Robert B. Innis, Molecular Imaging Branch, National Institute of Mental Health, 31 Center Dr., Bethesda, MD 20892-2035.
E-mail: robert.innis@nih.gov

The efflux transporter P-glycoprotein (P-gp) is widely distributed in the body and tends to decrease drug absorption from the intestine, increase elimination via the liver and kidneys, and block distribution to protected tissues such as the brain and testes (*1*). Several radiotracers, usually developed from drugs known to be substrates for P-gp, have been used to image the in vivo function of P-gp (*2–9*). Sestamibi was the first radiotracer used to image P-gp function (*8*) and was labeled with ^{99m}Tc for SPECT and ^{94m}Tc for PET. In addition to measuring the overexpression of P-gp in multidrug-resistant cancer, $^{99m/94m}$Tc-sestamibi is useful in measuring the function of P-gp at the blood–brain barrier, as demonstrated in P-gp knockout mice. Because of the high-energy emissions of ^{94m}Tc and the subsequent decay of daughter radionuclides, other radiotracers were developed for PET and labeled with ^{11}C or ^{18}F. These radiotracers, including ^{11}C-loperamide, ^{11}C-verapamil, and ^{18}F-paclitaxel, generate brain-penetrant radiometabolites that obscure the chemical source of the radioactive emissions from the brain.

Loperamide is used to treat diarrhea and acts on μ-opiate receptors in the intestine. Loperamide has virtually no central opiate effects, because P-gp avidly blocks its entry into the brain. After reports from others (*7,10,11*), we studied both ^{11}C-loperamide and ^{11}C-*N-desmethyl*-loperamide (^{11}C-dLop) in mice and monkeys as measures of P-gp function (*4,9,12*). As expected, both radioligands were avid substrates and had high brain uptake after the inactivation of P-gp by either genetic knockout or pharmacologic

inhibition. However, an injection of ^{11}C-loperamide led to the accumulation of significant concentrations of radiometabolites, including ^{11}C-dLop, in the brain. In contrast, an injection of ^{11}C-dLop itself markedly reduced radiometabolites in the brain.

Our animal studies showed that ^{11}C-dLop fulfills the 2 primary requirements for a radiotracer to measure P-gp function at the blood–brain barrier. That is, brain uptake is high after P-gp blockade, and most radioactivity in the brain reflects that of the parent radiotracer. The purposes of this study were to determine whether ^{11}C-dLop was a substrate for P-gp at the blood–brain barrier in humans and to measure the distribution of radioactivity in the entire body to estimate radiation exposure.

MATERIALS AND METHODS

Radiotracer Preparation

^{11}C-dLop was prepared by the methylation of the primary amide precursor with ^{11}C-iodomethane (*4*). The preparations were conducted according to our investigational new drug application (101,092), submitted to the U.S. Food and Drug Administration (http://pdsp.med.unc.edu/snidd/). The radiotracer was obtained in high radiochemical purity (100%) and with a specific activity of 93 ± 31 GBq/μmol (n = 12 batches) at the time of injection.

Human Subjects

Twelve healthy volunteers participated in the study (8 women, 4 men; age, 26 ± 3 y; body weight, 69 ± 13 kg). All subjects were free of current medical and psychiatric illness on the basis of history, physical examination, electrocardiogram, urinalysis (including drug screening), and blood tests. The subjects' vital signs were recorded before ^{11}C-dLop injection and at 15, 30, and 60 or 90 min after injection. Approximately 24 h after the PET scan, subjects returned to repeat urinalysis and blood tests.

PET

Brain Imaging. After the injection of ^{11}C-dLop (730 ± 16 MBq) in 4 subjects, PET scans were acquired for 60 (n = 2) or 90 (n = 2) min in 21 or 27 frames, respectively. PET scans were acquired in 3-dimensional mode with the High Resolution Research Tomograph (Siemens/CPS). Before radiotracer injection, a 6-min transmission scan was collected using a ^{137}Cs point source for attenuation correction.

Whole-Body Imaging. After the injection of ^{11}C-dLop (744 ± 5 MBq) in 8 subjects, whole-body PET scans were acquired in 2-dimensional mode on 7 segments of 15 cm each, from the head to the upper thigh, using an Advance tomograph (GE Healthcare). The total scanning time was approximately 120 min, with frames of 4 × 15 s, 3 × 30 s, 3 × 1 min, 3 × 2 min, and 1 × 4 min for each of the 7 body sections. Before radiotracer injection, a 32-min transmission scan of the 7 segments of the body was collected using a ^{68}Ge rod source for attenuation correction.

Measurement of ^{11}C-dLop in Plasma

Blood samples (1.5 mL each) were drawn from the radial artery at 15-s intervals until 120 s, followed by 1.5-mL samples drawn at 3, 5, and 10 min, 3-mL samples at 20 and 30 min, and 4.5-mL samples at 45, 60, 75, and 90 min. The plasma time–activity curve was corrected for the fraction of unchanged radiotracer, as previously described (*13*). The free fraction of ^{11}C-dLop in plasma was measured by ultrafiltration through membrane filters (Centrifree; Millipore), as previously described (*14*).

Image Analysis and Calculation of Outcome Measures

Brain Imaging. PET and MR images were coregistered using Statistical Parametric Mapping 2 (Wellcome Department of Cognitive Neurology). PET images of the entire scanning session were summed together to more clearly delineate brain and venous sinuses. Five regions of interest encompassing the entire brain, pituitary gland, venous sinuses, fourth ventricle, and choroid plexus were drawn on the coregistered MR image and mapped onto the PET images. Time–activity curves were expressed as percentage standardized uptake value (%SUV), which normalizes for injected activity and body weight: (% injected activity/cm^3 tissue) × (g body weight). Image and kinetic analyses were performed using pixelwise modeling software (PMOD 2.85; PMOD Technologies Ltd.).

Time–activity data were analyzed with 1- and 2-tissue-compartment models, using the radiometabolite-corrected plasma input function. To correct the brain data for its vascular component, radioactivity in serial whole blood was measured and then subtracted from the PET measurements, assuming that cerebral blood volume was 5% of the total brain volume.

Whole-Body Imaging. Whole-body tomographic PET images were compressed into a single planar image, and regions of interest were drawn on the following source organs that could be identified: thyroid, brain, heart, liver, lungs, kidneys, spleen, lumbar vertebrae, and urinary bladder. Because the lumbar vertebrae contain approximately 12.3% of the red marrow in an adult, this source organ was used as an approximation for uptake in the red marrow (*15*).

At each time point, the activities of identifiable source organs were converted into the fraction of the total injected activity. The area under the curve of each organ was calculated by the trapezoidal method to the end of imaging (~120 min). The area after the last time point to infinity was calculated by assuming that further decline occurred by physical decay only, without any biologic clearance. The area under the curve of percentage injected activity from time zero to infinity is equal to the residence time of the organ.

The mean total radioactivity in the urinary bladder was fitted with an exponential curve to estimate the percentage of injected activity excreted via this route. The dynamic bladder model, with a 2.4-h voiding interval, was implemented in OLINDA/EXM (version 1.0) to calculate organ-absorbed doses (*16*).

The organ values of injected activity were corrected for recovery of measured activity by placing a large region of interest over the entire body for each of the 14 frames. The injected activity of each source organ at every time point was corrected for recovery by multiplying by 100/X, where X is the measured recovery for the individual frame. The average recovery of all frames in 8 subjects was approximately 92%. If no radioactivity is lost to excretion, the total of all residence times equals $T_{1/2}/\ln(2)$, where $T_{1/2}$ = 20.4 min = 0.34 h, and $T_{1/2}/\ln(2)$ = 0.49 h. The residence time of the remainder of the body for each subject was calculated as 0.49 h minus the sum of the residence times of the source organs.

Group data are expressed as mean ± SD.

RESULTS

Minimal Brain Uptake of ^{11}C-dLop

After the injection of ^{11}C-dLop, uptake of radioactivity in the whole brain, including its vascular component, was low (<50% SUV; Figs. 1 and 2A). Uptake in the brain tissue itself, corrected for blood radioactivity, achieved concentrations of only approximately 15% SUV by 15–20 min and was stable until the end of the scanning session (60 min in 2 subjects and 90 min in the other 2 subjects). This low uptake of approximately 15% SUV in the brain from the 4 subjects who had dedicated brain imaging was confirmed in the 8 subjects who had whole-body imaging (Fig. 2B). In contrast to the low uptake in the brain, high concentrations of radioactivity accumulated in the pituitary and choroid plexus, about 650% and 280% SUV, respectively (Fig. 3). Uptake in the pituitary and choroid plexus, similar to that in the brain, was relatively rapid and stable until the end of the scanning session (90 min). However, because of the limited resolution of the PET images, we could not discern further whether the uptake was in the anterior pituitary (inside the blood–brain barrier) or in the posterior pituitary (outside the blood–brain barrier).

Uptake in the choroid plexus and venous sinus were visible on the tomographic images (Fig. 1) but were even more apparent in rotating 3-dimensional images of the brain acquired during the first 10 min (Supplemental Video 1; supplemental materials are available online only at http://jnm.snmjournals.org).

To determine whether uptake in the choroid plexus was subsequently excreted into the cerebral spinal fluid (CSF), we compared the time course of radioactivity in the choroid plexus and fourth ventricle. In fact, activity accumulated in the choroid plexus (i.e., increased from zero activity to a stable plateau of about 280% SUV), whereas activity in the CSF of the fourth ventricle declined from an early peak to a low stable level of about 10% SUV. Thus, uptake in the choroid plexus appeared to be trapped in this tissue and showed no evidence of excretion into the CSF.

Overall, radioactivity in regions within the skull reflected 2 general sources: blood pool (the whole brain; venous sinus) and accumulation in tissues (the brain itself, pituitary, and choroid plexus). Of course, the time course of radioactivity in the blood pool reflected that in plasma—a rapid peak, followed by a rapid decline. Thus, the whole brain and venous sinus had an early peak, followed by a rapid washout. In contrast, the brain itself, pituitary, and choroid plexus increased to a plateau. However, radioactivity in all 5 regions (the whole brain, brain corrected for vascular component, venous sinus, pituitary, and choroid plexus) were relatively stable for the terminal portion of the scan.

Plasma Clearance

The average concentration of ^{11}C-dLop in plasma peaked at approximately 1 min and decreased rapidly in 4 subjects (Fig. 4). The concentrations after this peak were fitted well

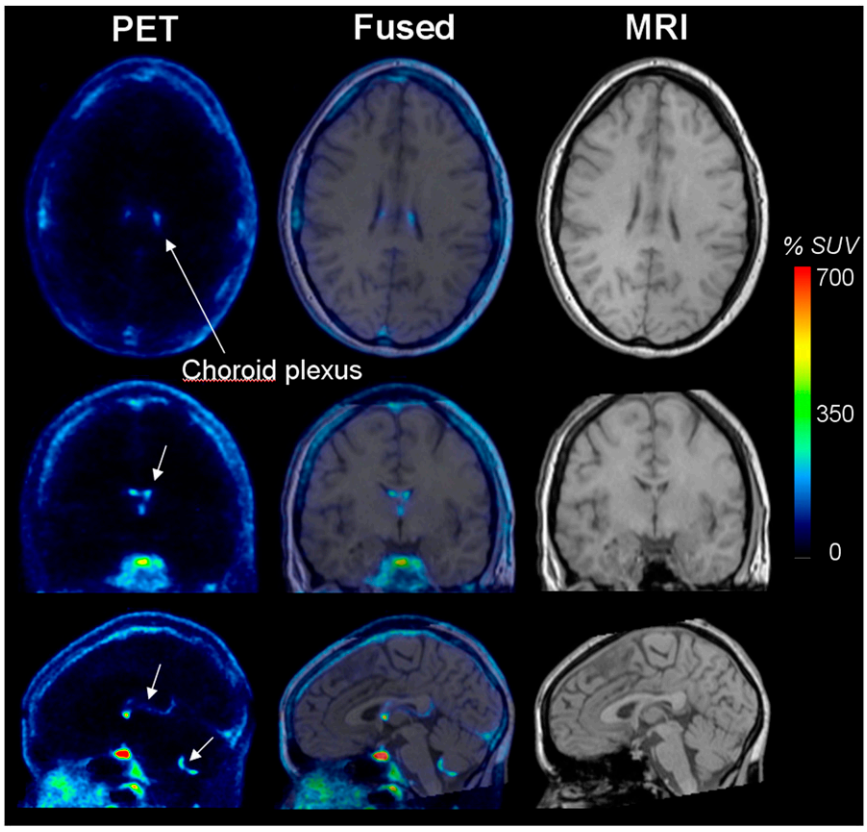

RGB

FIGURE 1. PET images of ^{11}C-dLop in human brain and corresponding MR image. PET images were summed from 0 to 90 min, and pixel values represent mean concentration of radioactivity (%SUV). Coregistered MR images and fused PET and MR images are also shown. Arrows point to choroid plexus on medial surfaces of lateral ventricles and on roof of third and fourth ventricles.

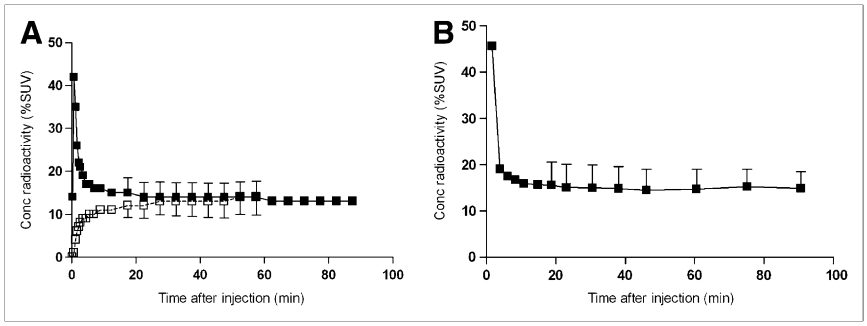

FIGURE 2. (A) Concentration of radioactivity in brain, with (□) and without (■) vascular correction, in 4 subjects who had head-dedicated imaging. Symbols represent mean values. SD bars are included for all points after 18 min. Note that SD bars are smaller than symbols for all points after 60 min. (B) Concentration of radioactivity in brain in 8 subjects who had whole-body imaging. Vascular correction of brain activity could not be performed in these subjects, because no blood was collected during scanning. Conc = concentration.

with a biexponential function and had mean half-lives of 0.4 and 15 min. Calculated as the partial areas under the concentration–time curve, these 2 half-lives accounted for 40% and 60% of the total area under the curve from peak to infinity.

The fraction of ^{11}C-dLop, expressed as a percentage of total plasma activity, comprised a stable and high percentage (85%) of total radioactivity from 5 min to the end of the scan (Fig. 5A). Five radiometabolite peaks were detected in arterial plasma samples with high-performance liquid chromatography (Fig. 5B). All 5 radiometabolites peaked earlier than did the parent radiotracer and were, therefore, less lipophilic than dLop. The plasma-free fraction of ^{11}C-dLop was 11.4% ± 3.3% in 4 subjects.

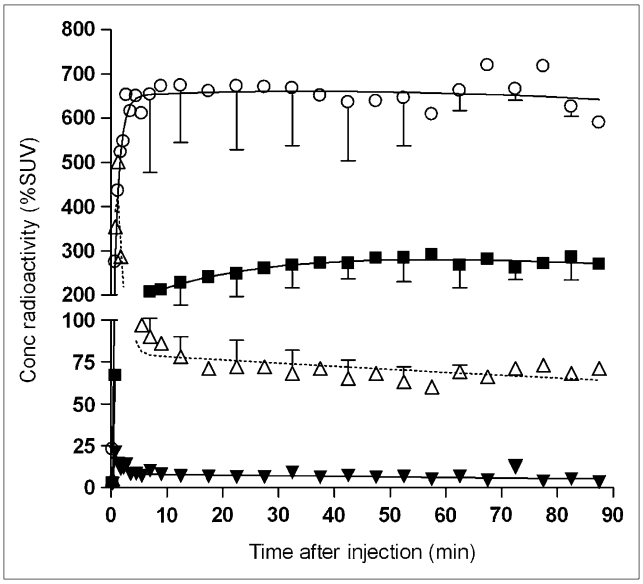

FIGURE 3. After injection of ^{11}C-dLop, radioactivity in pituitary gland (○) and choroid plexus (■) peaked quickly and remained stable during course of scan, whereas uptake in venous sinus (△) and fourth ventricle (i.e., CSF) (▼) peaked quickly and stabilized at lower level. Symbols represent mean values in 4 subjects. For clarity, SD bars are included only after 5 min and for every other time point. Conc = concentration.

Kinetic Analysis

Compartmental modeling of whole brain time–activity data and serial concentrations of plasma ^{11}C-dLop were poorly fit by a 1-tissue-compartment model and did not converge with a 2-tissue-compartment model. For the 1-tissue-compartment model, the rate of entry (K_1) of radiotracer into the brain was poorly identified (~30%), and k_2 was essentially not identified (>1,000%). As expected from the low brain uptake, the rate constant K_1 was only 0.009 ± 0.002 mL·cm^{-3}·min^{-1} (mean ± SD in 4 subjects). Because the stable uptake in the brain suggested an irreversible process, we also fitted brain data with k_2 set to 0. This constraint insignificantly affected the value of K_1.

Whole-Body Biodistribution

The lungs, liver, spleen, thyroid, urinary bladder, and kidneys were easily identified as source organs on the whole-body images (Fig. 6). The lungs had the highest uptake of radioactivity, with a peak value of 33% at approximately 2 min (Fig. 7). The liver also exhibited high uptake, which continuously increased for the duration of the scan to 22% injected activity at approximately 100 min (Fig. 7A). Uptake in the liver increased approximately 1.5-fold, from 20 min to the end of the scan. Uptake in the brain peaked quickly and leveled off at 0.03% injected activity, from 3 min to the end of the scan (Fig. 7B). The mean cumulative urine activity was well fitted (r^2 = 0.92), with an exponential curve (data not shown). The exponential fitting had an asymptote of approximately 4% of injected activity at time of infinity, indicating that only approximately 4% injected activity was excreted by the urinary route. The whole-body images in Figure 6 use a format (maximal intensity projection) that emphasizes anatomy with high radioactivity uptake but may cause visual misperception of the total radioactivity (e.g., in the urinary bladder). Although they are difficult to visualize on the maximal-intensity-projection images (Fig. 6), the horizontal and midsagittal sinuses were easily seen on rotating 3-dimensional images at early times (0–10 min) after the injection of ^{11}C-dLop (Supplemental Video 1).

Human residence times were estimated using average values from the planar images (Table 1). The organs with

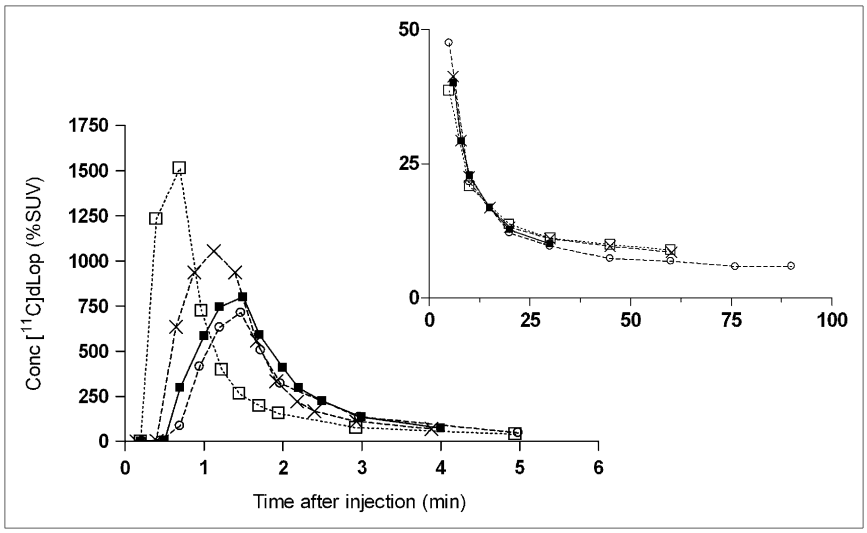

FIGURE 4. Concentration of unchanged ^{11}C-dLop in plasma after radiotracer injection. Curve is shown with 2 time intervals (0–5 min and 5–90 min) because of high concentrations at early time points. Each symbol represents 1 of the 4 healthy control subjects. Conc = concentration.

the highest radiation burden (μSv/MBq) were the kidneys (50.1), spleen (30.5), and lungs (27.0) (Table 2). With a 2.4-h voiding interval, the effective dose was 7.8 ± 0.6 μSv/MBq (28.7 ± 2.2 mrem/mCi; mean ± SD in 8 subjects).

DISCUSSION

^{11}C-dLop has minimal uptake in the healthy human brain. The low brain uptake of radioactivity (~15% SUV) confirms that minimal amounts of radiometabolites (and parent radiotracer) enter the brain. The low rate of brain entry (K_1 = 0.009 mL·cm^{-3}·min^{-1}) is consistent with ^{11}C-dLop being a substrate for P-gp, which blocks entry of compounds rather than enhances removal. As a measure of radiation exposure to the entire body, the effective dose of ^{11}C-dLop was 7.8 ± 0.6 μSv/MBq. The mass dose of carrier *N*-dLop (4.1 ± 1.5 μg) injected with ^{11}C-dLop produced no subjective effects and no significant changes in laboratory tests, electrocardiogram, blood pressure, pulse, or respiration rate. Therefore, ^{11}C-dLop appears safe from both a pharmacologic and a radiologic perspective.

Comparison with ^{11}C-Verapamil

^{11}C-verapamil is the radiotracer that has been most extensively studied as an agent for measuring P-gp function at the blood–brain barrier. ^{11}C-verapamil generates more brain-penetrant radiometabolites than does ^{11}C-dLop in rats and possibly also in humans. At 30 min after injection in rats, approximately 30% of brain radioactivity is caused by radiometabolites for ^{11}C-verapamil (*17*), compared with less than 10% for ^{11}C-dLop (*4*). ^{11}C-verapamil likely generates radiometabolites in humans, as suggested by a 4-fold higher brain uptake in healthy subjects in ^{11}C-verapamil studies versus the brain uptake in subjects in ^{11}C-dLop studies (70% vs. 15% SUV, respectively) (*18*). Consistent with its greater brain uptake, the K_1 of ^{11}C-verapamil (0.05 mL·cm^{-3}·min^{-1}) is about 5-fold greater than that of ^{11}C-dLop (0.009 mL·cm^{-3}·min^{-1}).

The metabolism of ^{11}C-dLop in humans had one unexpected finding; namely, ^{11}C-dLop comprised a stable and high percentage (85%) of total radioactivity from 5 min to the end of the scan. Our prior study of ^{11}C-dLop in the monkey showed the more typical pattern in which the percentage composition of parent radiotracer declines over time. The percentage of radioactivity that was ^{11}C-dLop in monkey plasma declined from 100% at time 0 to 50% at 40 min (*4*). The high percentage composition of human plasma by ^{11}C-dLop may help ensure that few radiometabolites enter the brain. Furthermore, the radiometabolites in both human and monkey plasma eluted earlier than the parent radiotracer and were, therefore, less lipophilic than dLop (Fig. 5B). In fact, the major radiometabolite (A in Fig. 5B) was the least lipophilic (Fig. 5B) and, therefore, the least likely to enter the brain.

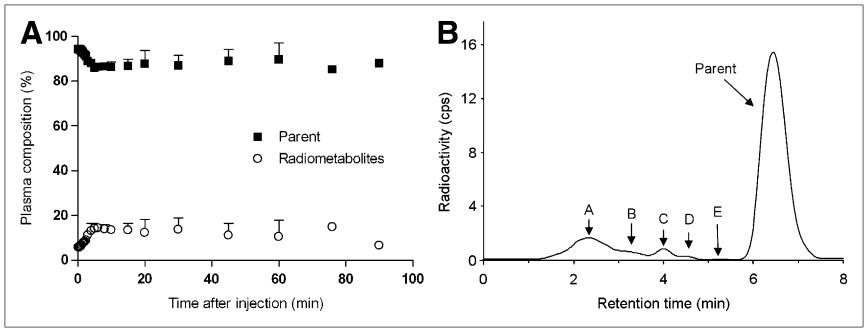

FIGURE 5. (A) Percentage composition of plasma radioactivity over time is shown for ^{11}C-dLop (■) and total radiometabolites (○) (n = 4 subjects). Symbols represent mean ± SD, although SD is sometimes smaller than size of symbol. (B) Representative radiochromatogram of plasma at 30 min after injection of ^{11}C-dLop. Parent constituted 88% of total radioactivity. Radiometabolites (A–E) are less lipophilic than ^{11}C-dLop. cps = counts per second.

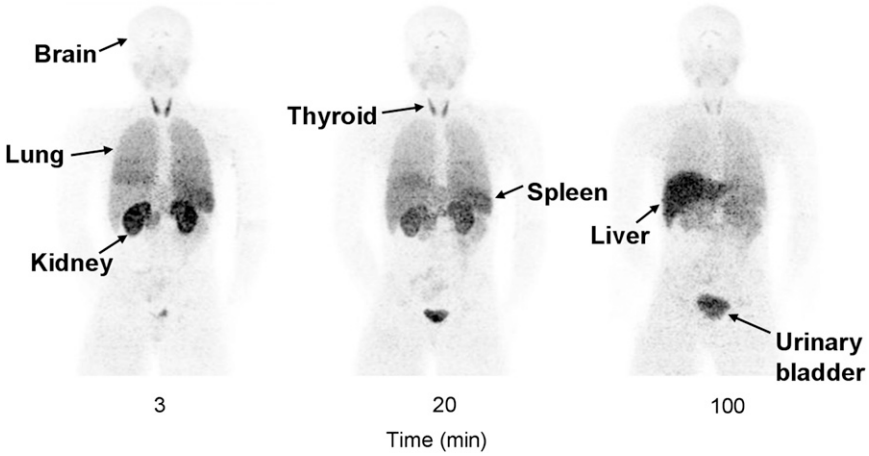

FIGURE 6. Maximal-intensity-projection images of distribution of radioactivity in healthy male subject at 3, 20, and 100 min after injection of ^{11}C-dLop.

Radiation Dosimetry and Whole-Body Imaging

The radiation exposure of ^{11}C-dlop (7.8 μSv/MBq) was similar to that of many other ^{11}C-radiotracers (range, ~4.3–14.1 μSv/MBq) and was, therefore, an expected finding (*19*). After the injection of ^{11}C-dLop, both the thyroid and the pituitary had a high uptake of radioactivity in humans (current study) and in monkeys (*4,12*). The dosimetry software (OLINDA/EXM) (*16*) calculates exposure to the thyroid but not to the pituitary (Table 2). To estimate exposure to the pituitary, we assumed that its concentration of radioactivity was constant at 650% SUV (Fig. 2) and that its weight was 0.6 g. The pituitary dose was 12.4 μSv/MBq injected activity, assuming the pituitary was a small sphere such that the dose to the organ was only from activity in the organ itself. This value would be an overestimation if the radioactivity was derived from a volume larger than the pituitary itself, which we cannot determine with the resolution of the PET scans. Nevertheless, this estimated radiation exposure to the pituitary is similar to that to the liver (12.9 μSv/MBq) but much less than that to the kidney (50.1 μSv/MBq), which had the highest radiation exposure.

Another surprising finding was the prominent visualization of the system of venous sinuses surrounding the brain. Although difficult to discern on the coronal images (Fig. 6), the horizontal and midsagittal sinuses were easily seen on sagittal or rotating 3-dimensional images at early times (0–10 min) after the injection of the radiotracer (Supplemental Video 1). The sinuses were easily visualized because the adjacent brain had negligible radioactivity.

Finally, in this study we estimated radiation dosimetry exposure using 2-dimensional planar images that have been found to provide conservative estimates of radiation exposure. We previously compared radiation exposure estimated with 2-dimensional planar, bisected, and thin-slice tomographic images using the phosphodiesterase 4 radiotracer ^{11}C-(*R*)-rolipram and substance P (NK_1) receptor radiotracer ^{18}F-SPA-RQ (*20,21*). In both studies, planar and bisected images provided organ dose estimates similar to, but slightly higher than, those of thin-slice images.

CONCLUSION

The low uptake of radioactivity in the brain is consistent with ^{11}C-dLop being a substrate for P-gp in humans and confirms that this radiotracer generates negligible quantities of brain-penetrant radiometabolites. The K_1 is consistent with P-gp rapidly effluxing substrates while they transit through the lipid bilayer. The radiation exposure of ^{11}C-dLop is similar to that of many other ^{11}C radiotracers and would allow multiple PET scans per year in the same subject. ^{11}C-dLop is a promising radiotracer to study the function of P-gp at the blood–brain barrier, at which impaired function would allow increased uptake into the brain.

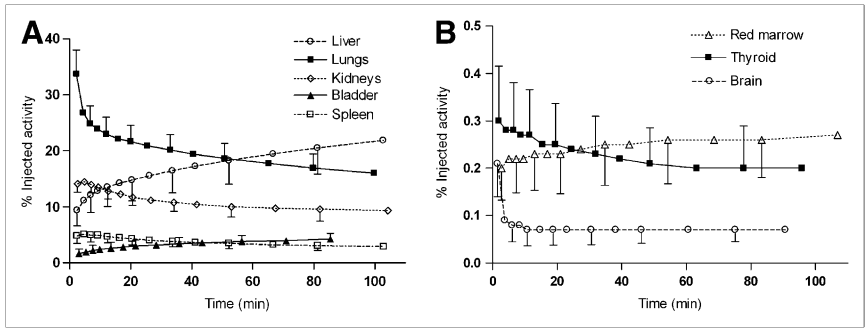

FIGURE 7. Uptake of radioactivity in organs that could be visually identified on planar whole-body images. Activity of organ is expressed as percentage of injected activity. Data are mean ± SD in 8 subjects.

TABLE 1. Residence Times of Source Organs

Source organ	Residence time (h)
Thyroid	0.001 ± 0.000
Brain	0.002 ± 0.001
Lungs	0.102 ± 0.014
Liver	0.068 ± 0.017
Urinary bladder	0.013 ± 0.005
Spleen	0.019 ± 0.005
Kidneys	0.055 ± 0.007
Red marrow	0.009 ± 0.003
Remainder in body	0.220 ± 0.007

Data are mean ± SD.

ACKNOWLEDGMENTS

We thank the staff of the NIH PET Department for successfully performing the PET studies, Edward Tuan for assistance with the blood samples, Maria Ferraris Araneta, CRNP, for subject recruitment and care, and PMOD Technologies (Zurich, Switzerland) for providing its image-analysis and modeling software. A patent application has been filed on behalf of the U.S. government for PET imaging of P-gp function; Drs. Sami Zoghbi, Victor Pike, and Robert Innis could personally benefit from this patent.

TABLE 2. Radiation Dosimetry Estimates for ^{11}C-dLop Determined from 8 Healthy Subjects

Target organ doses	μSv/MBq	mrem/mCi
Adrenals	4.2 ± 0.1	15.4 ± 0.4
Brain	0.8 ± 0.2	2.9 ± 0.7
Breasts	2.0 ± 0.1	7.5 ± 0.2
Gallbladder wall	3.8 ± 0.3	14.1 ± 1.1
LLI wall	1.9 ± 0.1	7.2 ± 0.4
Small intestine	2.3 ± 0.1	8.5 ± 0.2
Stomach	2.8 ± 0.1	10.3 ± 0.3
ULI wall	2.3 ± 0.1	8.7 ± 0.3
Heart wall	3.2 ± 0.1	11.8 ± 0.3
Kidneys	50.1 ± 6.0	184.9 ± 22
Liver	12.9 ± 2.7	47.9 ± 10
Lungs	27.0 ± 3.4	99.8 ± 13
Muscle	2.0 ± 0.0	7.3 ± 0.1
Ovaries	2.0 ± 0.1	7.5 ± 0.4
Pancreas	4.0 ± 0.2	14.9 ± 0.6
Red marrow	2.9 ± 0.3	10.9 ± 1.1
Osteogenic cells	3.0 ± 0.2	11.2 ± 0.7
Skin	1.4 ± 0.0	5.3 ± 0.1
Spleen	30.5 ± 6.8	112.7 ± 25
Testes	1.5 ± 0.1	5.5 ± 0.3
Thymus	2.3 ± 0.1	8.6 ± 0.3
Thyroid	14.7 ± 6.2	54.5 ± 23
Urinary bladder wall	10.8 ± 3.3	39.8 ± 12
Uterus	2.2 ± 0.2	8.3 ± 0.7
Total body	2.9 ± 0.0	10.8 ± 0.1
Effective dose	7.8 ± 0.6	28.7 ± 2.2

LLI = lower large intestine; ULI = upper large intestine.
Data are mean ± SD.

The Intramural Research Program of NIMH supported this research (project Z01-MH-002852-04).

REFERENCES

1. Fromm MF. Importance of P-glycoprotein at blood-tissue barriers. *Trends Pharmacol Sci.* 2004;25:423–429.
2. Bigott HM, Prior JL, Piwnica-Worms DR, Welch MJ. Imaging multidrug resistance P-glycoprotein transport function using microPET with technetium-94m-sestamibi. *Mol Imaging.* 2005;4:30–39.
3. Kurdziel KA, Kiesewetter DO, Carson RE, Eckelman WC, Herscovitch P. Biodistribution, radiation dose estimates, and in vivo Pgp modulation studies of ^{18}F-paclitaxel in nonhuman primates. *J Nucl Med.* 2003;44:1330–1339.
4. Lazarova N, Zoghbi S, Hong J, et al. Synthesis and evaluation of [*N-methyl*-^{11}C]*N-desmethyl*-loperamide as a new and improved PET radiotracer for imaging P-gp function. *J Med Chem.* 2008;51:6034–6043.
5. Lee YJ, Maeda J, Kusuhara H, et al. In vivo evaluation of P-glycoprotein function at the blood-brain barrier in nonhuman primates using [^{11}C]verapamil. *J Pharmacol Exp Ther.* 2006;316:647–653.
6. Lubberink M, Luurtsema G, van Berckel BN, et al. Evaluation of tracer kinetic models for quantification of P-glycoprotein function using (*R*)-[^{11}C]verapamil and PET. *J Cereb Blood Flow Metab.* 2007;27:424–433.
7. Passchier R, Comley R, Salinas C, et al. The role of P-glycoprotein on blood brain barrier permeability of ^{11}C-loperamide in humans [abstract]. *Neuroimage.* 2008;41(suppl 2):T192.
8. Piwnica-Worms D, Chiu ML, Budding M, Kronauge JF, Kramer RA, Croop JM. Functional imaging of multidrug-resistant P-glycoprotein with an organotechnetium complex. *Cancer Res.* 1993;53:977–984.
9. Zoghbi SS, Liow JS, Yasuno F, et al. ^{11}C-loperamide and its *N-desmethyl* radiometabolite are avid substrates for brain permeability-glycoprotein efflux. *J Nucl Med.* 2008;49:649–656.
10. Passchier J, Bender D, Mattews JC, Lawrie KW, Gee AD. ^{11}C-loperamide: a novel and sensitive PET probe for quantification of changes in P-glycoprotein functionality [abstract]. *Mol Imaging Biol.* 2003;5:121.
11. Wilson A, Passchier J, Garcia A, et al. Production of the P-glycoprotein marker, [^{11}C]loperamide, in clinically useful quantities [abstract]. *J Labelled Comp Radiopharm.* 2005;48(suppl):S142.
12. Liow JS, Kreisl W, Zoghbi SS, et al. P-glycoprotein function at the blood-brain barrier imaged using ^{11}C-*N*-desmethyl-loperamide in monkeys. *J Nucl Med.* 2009;50:108–115.
13. Zoghbi SS, Shetty UH, Ichise M, et al. PET imaging of the dopamine transporter with ^{18}F-FECNT: a polar radiometabolite confounds brain radioligand measurements. *J Nucl Med.* 2006;47:520–527.
14. Gandelman MS, Baldwin RM, Zoghbi SS, Zea-Ponce Y, Innis RB. Evaluation of ultrafiltration for the free-fraction determination of single photon emission computed tomography (SPECT) radiotracers: β-CIT, IBF, and iomazenil. *J Pharm Sci.* 1994;83:1014–1019.
15. Valentin J. *Basic Anatomical and Physiological Data for Use in Radiological Protection: Reference Values.* ICRP Publication 89. Oxford, U.K.: Pergamon Press; 2001:167–185.
16. Stabin MG, Sparks RB, Crowe E. OLINDA/EXM: the second-generation personal computer software for internal dose assessment in nuclear medicine. *J Nucl Med.* 2005;46:1023–1027.
17. Luurtsema G, Molthoff CF, Schuit RC, Windhorst AD, Lammertsma AA, Franssen EJ. Evaluation of (*R*)-^{11}C-verapamil as PET tracer of P-glycoprotein function in the blood-brain barrier: kinetics and metabolism in the rat. *Nucl Med Biol.* 2005;32:87–93.
18. Ikoma Y, Takano A, Ito H, et al. Quantitative analysis of ^{11}C-verapamil transfer at the human blood-brain barrier for evaluation of P-glycoprotein function. *J Nucl Med.* 2006;47:1531–1537.
19. Brown AK, Fujita M, Fujimura Y, et al. Radiation dosimetry and biodistribution in monkey and man of ^{11}C-PBR28: a PET radioligand to image inflammation. *J Nucl Med.* 2007;48:2072–2079.
20. Sprague DR, Chin FT, Liow JS, et al. Human biodistribution and radiation dosimetry of the tachykinin NK1 antagonist radioligand [^{18}F]SPA-RQ: comparison of thin-slice, bisected, and 2-dimensional planar image analysis. *J Nucl Med.* 2007;48:100–107.
21. Sprague DR, Fujita M, Ryu YH, Liow JS, Pike VW, Innis RB. Whole-body biodistribution and radiation dosimetry in monkeys and humans of the phosphodiesterase 4 radioligand [^{11}C]-(*R*)-rolipram: comparison of two-dimensional planar, bisected and quadrisected image analyses. *Nucl Med Biol.* 2008;35:493–500.